J Mater Sci (2007) 42:8853–8863
DOI 10.1007/s10853-007-1812-6

A polyconvex hyperelastic model for fiber-reinforced materials in application to soft tissues

Alexander E. Ehret · Mikhail Itskov

Received: 15 December 2006 / Accepted: 30 April 2007 / Published online: 12 August 2007

Abstract In this paper a generalized anisotropic hyperelastic constitutive model for fiber-reinforced materials is proposed. Collagen fiber alignment in biological tissues is taken into account by means of structural tensors, where orthotropic and transversely isotropic material symmetries appear as special cases. The model is capable to describe the anisotropic stress response of soft tissues at large strains and is applied for example to different types of arteries. The proposed strain energy function is polyconvex and coercive. This guarantees the existence of a global minimizer of the total elastic energy, which is important in the context of a boundary value problem.

Introduction

In soft biological tissues the distribution, arrangement and interaction of the constituents lead to a diversity of mechanical characteristics and thus high specificity and functionality. In particular, the extracellular matrix plays an important role. Its main constituents are proteins, glycosaminoglycans as well as bound and unbound water, see e.g., [1]. Among those proteins, different collagen types are crucial for the mechanical properties of soft tissues. Indeed, some collagen types form fibers or networks and thus provide reinforcing structures. By ordered arrangement, this finally leads to anisotropy. The alignment of these structures is manifold and reaches from parallel fiber bundles in tendons to helical arrangement in arteries and two- and three-dimensional networks in skin, see e.g., [2]. Collagen fibers are usually crimped or undulated in a natural state. With increasing strain they line-up, straighten, and finally become the main load bearing elements. As a consequence, the stress response of soft tissue samples is in general characterized by highly non-linear behavior with *J*-shaped or nearly exponential stress-strain curves. Hence, from a biomechanical perspective, both anisotropy and non-linear behavior at large elastic strains should be regarded by a constitutive model in order to describe soft tissues appropriately. In the elastic domain, hyperelastic models meet these requirements and have therefore extensively been utilized in soft tissue mechanics.

The diversity among the mechanical characteristics of soft tissues motivated a great number of constitutive formulations for different tissue types. For example, the reader is referred to [3] for a survey on strain energy functions for planar biological tissues in connection with biaxial testing techniques. Modeling approaches for various components of the cardiovascular system the reader may find in [1] and references therein. In particular, arterial wall mechanics as well as several hyperelastic models for arterial tissue are studied in [4]. Several strain energy functions for myocardium have recently been compared by Schmid et al. [5]. Although the major part of these models is based on phenomenological approaches, a number of micromechanically based models have been suggested. For example, chain network models (see e.g., [6]), taking into account single collagen fibrils by means of statistical mechanics, have been applied to model orthotropic and transversely isotropic soft tissues [7, 8]. Other authors derived constitutive relations based on sinusoidal, zig-zag or circular helix representations for the crimped collagen fibers, see e.g., [9–11]. The material parameters appearing in microstructurally based models generally have a

A. E. Ehret (✉) · M. Itskov
Department of Continuum Mechanics, RWTH Aachen University, Eilfschornsteinstr. 18, 52062 Aachen, Germany
e-mail: ehret@km.rwth-aachen.de

physical meaning. However, estimation of these parameters might be a difficult task in view of the variance among individual tissue samples. In general, phenomenological models are able to adequately describe the macroscopic behavior of soft tissues observed in experiments and have therefore wide applicability. Although the related material parameters do not usually provide a clear physical interpretation, they can be obtained by fitting the model to experimental data. Notwithstanding, even within a phenomenological approach it is preferable to include as much information about the structure as possible. Thus, motivated by the histological structure of blood vessels, Holzapfel et al. [4] considered each layer of an arterial wall as a fiber-reinforced composite of an isotropic matrix and two symmetrically arranged fiber helices. This led to a multi-layer constitutive model with an elastic potential composed of an isotropic part and an anisotropic part associated with the two fiber contributions. In a recent paper, Gasser et al. [12] have presented an approach to replace the mean fiber directions in the latter model by a collagen fiber dispersion as experimentally observed by means of polarized light microscopy.

Besides these biomechanical aspects, the issue of material stability should be taken into account if the tissue is assumed to maintain its integrity throughout the elastic deformations. Possible criteria for material stability have recently been discussed [13]. One of those is the strong ellipticity condition, which also implicates positive definiteness of the acoustic tensor so that the speed of displacement waves is real for any direction of propagation. Contrariwise, the loss of ellipticity has recently been used to describe several failure mechanisms in fiber-reinforced materials like, e.g., fiber kinking, splitting and de-bonding [14, 15]. Investigation of ellipticity for several constitutive models (see e.g., [16]) showed, for example, that the so-called Fung elastic model [2, 17] widely and successfully applied to soft biological tissues is in general not elliptic and that enforcement of the strong ellipticity condition imposes severe restrictions on the material constants. For polyconvex strain energy functions [18] on the other hand, ellipticity is guaranteed (see e.g., [19]). Another advantage of polyconvex functions appears in the context of boundary value problems. The question whether there is a solution of the boundary value problem is bound to the existence of a global minimizer of the total elastic energy of a body. According to Ball [18, 20] this minimizer exists if the strain energy function is polyconvex and satisfies a certain growth condition referred to as coercivity. Hence, polyconvexity provides an excellent starting point to formulate strain energy functions that guarantee both ellipticity and existence of the global minimizer.

Instead of checking various anisotropic hyperelastic models for polyconvexity, one can formulate polyconvex strain energy functions from scratch. Schröder and Neff [19] investigated polyconvexity of numerous functions of isotropic and anisotropic strain invariants. On this basis, they proposed a variety of polyconvex free energy terms for a transversely isotropic material as well as an extension for orthotropic materials. Furthermore, for these material symmetries, sufficient conditions for the polyconvexity and coercivity of the strain energy function were elaborated by Steigmann [21]. Itskov and Aksel [22] presented a class of transversely isotropic and orthotropic polyconvex and coercive strain energy functions. An advantage of the latter formulation is that the functions fulfill the condition of an energy and stress-free undeformed configuration a priori. Their hyperelastic model is based on a power series representation with an arbitrary number of terms. A modified version of the model, based on an exponential function representation was successfully utilized to describe the mechanical behavior of soft collagenous tissues by Itskov et al. [23]. Balzani et al. [24] followed the approach by Holzapfel [4] and presented a number of polyconvex strain energies for soft biological tissues consisting of an isotropic part and the superposition of several transversely isotropic contributions. We remark that some of the material parameters in these models should be restricted further to prevent the initial stiffness associated with the fiber part from being infinite. In the models [4, 24], the transversely isotropic parts are switched off if the associated preferred directions are under compression. This guarantees convexity of the strain energy function, however, it leads to purely isotropic behavior when all fibers are in a compressive state.

In this paper we present a polyconvex anisotropic hyperelastic constitutive model for materials consisting of an isotropic matrix and reinforced by an arbitrary number of fiber families. Each fiber family is explicitly taken into account by a structural tensor and associated with a weight factor. The model is formulated in terms of so-called generalized structural tensors. It is shown that for a material reinforced by a single family of fibers, these tensors coincide with a recently proposed structure tensor that includes collagen fiber dispersion [12]. The model is developed in a generalized form offering maximum flexibility for use with different types of engineering materials and biological tissues. Earlier models for orthotropic and transversely isotropic materials are included as special cases.

The paper is organized as follows: We begin with the basic mathematical notations and definitions as well as a short discussion of hyperelasticity. Then, the generalized structural tensors and a functional basis for the anisotropic strain energy function are introduced. We proceed with the derivation of the generalized polyconvex and coercive strain energy function. Finally, numerical examples are presented, showing special cases of the model in application to arterial tissue.

Preliminaries

Basic tensor operations

Let **Lin** be a set of all linear mappings of a three-dimensional vector space $\mathbb{R}^3$ over reals into itself. **Lin** represents a finite-dimensional vector space with the inner product. The elements of **Lin** are called second-order tensors. Subsets of **Lin** are defined by $\mathbf{Sym} = \{\mathbf{M} \in \mathbf{Lin} : \mathbf{M} = \mathbf{M}^{\mathrm{T}}\}$, $\mathbf{Orth} = \{\mathbf{Q} \in \mathbf{Lin} : \mathbf{Q} = \mathbf{Q}^{-\mathrm{T}}\}$, and $\mathbf{Inv} = \{\mathbf{A} \in \mathbf{Lin} : \det\mathbf{A} \neq 0\}$, constituted by symmetric, orthogonal, and invertible second-order tensors, respectively, where $\det\mathbf{A}$ denotes the determinant of a second-order tensor $\mathbf{A}$. $\mathbf{Sym}^{+}$ is a subset of **Sym** formed by all positive definite symmetric second-order tensors. The adjugate of a second-order tensor is denoted by $\mathrm{adj}\mathbf{A} = \mathbf{A}^{-1}\det\mathbf{A}$ and the cofactor by $\mathrm{cof}\mathbf{A} = \mathbf{A}^{-\mathrm{T}}\det\mathbf{A}$, where $\mathbf{A} \in \mathbf{Inv}$.

Let $\mathbb{L}\mathrm{in}$ be a set of all linear mappings of **Lin** into itself so that $\mathbf{B} = \mathbb{D} : \mathbf{A}$, $\mathbf{B} \in \mathbf{Lin}$, $\forall \mathbf{A} \in \mathbf{Lin}$, $\forall \mathbb{D} \in \mathbb{L}\mathrm{in}$. The elements of $\mathbb{L}\mathrm{in}$ are called fourth-order tensors. They can be constructed from second-order tensors by means of the tensor products "$\odot$" and "$\otimes$" such that (see e.g., [25])

$$\begin{aligned} &\mathbf{A} \odot \mathbf{B} : \mathbf{C} = \mathbf{A}(\mathbf{B} : \mathbf{C}), \quad \mathbf{A} \otimes \mathbf{B} : \mathbf{C} = \mathbf{ACB}, \\ &\mathbf{A}, \mathbf{B} \in \mathbf{Lin}, \ \forall \mathbf{C} \in \mathbf{Lin}. \end{aligned} \tag{1}$$

Note that these definitions differ from notations in other works. A simple composition of fourth-order tensors with second-order ones is introduced by

$$(\mathbf{A}\mathbb{D}\mathbf{B}) : \mathbf{C} = \mathbf{A}(\mathbb{D} : \mathbf{C})\mathbf{B}, \quad \mathbb{D} \in \mathbb{L}\mathrm{in}, \mathbf{A}, \mathbf{B} \in \mathbf{Lin}, \quad \forall \mathbf{C} \in \mathbf{Lin}. \tag{2}$$

The calculation of stresses and elasticity tensors requires application of the derivative with respect to a tensor. This derivative obeys the following product rules of differentiation [26]

$$\begin{aligned} (f\mathbf{A})_{,\mathbf{C}} &= \mathbf{A} \odot f_{,\mathbf{C}} + f\mathbf{A}_{,\mathbf{C}}, \\ (\mathbf{AB})_{,\mathbf{C}} &= \mathbf{A}_{,\mathbf{C}}\mathbf{B} + \mathbf{AB}_{,\mathbf{C}}, \end{aligned} \tag{3}$$

where f, $\mathbf{A}$, and $\mathbf{B}$ represent a scalar and two tensor-valued differentiable tensor functions of $\mathbf{C}$, respectively. The notation $(\bullet)^{S}$ indicates a symmetrization operation on fourth-order tensors defined by (see e.g., [25])

$$\mathbb{D}^{S} : \mathbf{A} = \mathbb{D} : \frac{1}{2}\left(\mathbf{A} + \mathbf{A}^{\mathrm{T}}\right), \ \mathbb{D} \in \mathbb{L}\mathrm{in}, \ \forall \mathbf{A} \in \mathbf{Lin}. \tag{4}$$

A function f of several arguments, say $x_1, x_2, \ldots, x_n$, will be abbreviated by the notation $f = \hat{f}(x_i)$, $i = 1, 2, \ldots, n$.

Hyperelasticity

An elastic material is called hyperelastic if its elastic behavior can be described by a strain energy function $W = W_{\mathbf{F}}(\mathbf{F})$ per unit reference volume, where $\mathbf{F}$ denotes the deformation gradient. According to the principle of objectivity, the strain energy has to be independent of superposed rigid body motions. This requirement can automatically be satisfied representing the strain energy function in terms of the right Cauchy–Green tensor $\mathbf{C} = \mathbf{F}^{\mathrm{T}}\mathbf{F}$ so that

$$W = W_{\mathbf{F}}(\mathbf{F}) = W_{\mathbf{C}}(\mathbf{C}). \tag{5}$$

For an unconstrained hyperelastic material, a constitutive law can be given by (see e.g., [27])

$$\mathbf{S} = 2\frac{\partial W}{\partial \mathbf{C}}, \tag{6}$$

where $\mathbf{S}$ denotes the second Piola–Kirchhoff stress tensor. The material time derivative of Eq. (6) yields

$$\dot{\mathbf{S}} = \mathbb{C} : \frac{1}{2}\dot{\mathbf{C}}, \tag{7}$$

where $\mathbb{C}$ is the tangent tensor of fourth order defined by

$$\mathbb{C} = 2\frac{\partial \mathbf{S}}{\partial \mathbf{C}} = 4\frac{\partial^2 W}{\partial \mathbf{C}\partial \mathbf{C}}. \tag{8}$$

For constrained materials, the constitutive law takes the form

$$\mathbf{S} = 2\frac{\partial W}{\partial \mathbf{C}} + q\frac{\partial \zeta}{\partial \mathbf{C}}, \tag{9}$$

with an arbitrary scalar q and a function ζ accounting for the kinematic constraint $\zeta(\mathbf{C}) = 0$. Accordingly, the stress rate and the tangent tensor of fourth order are given by (see e.g., [28])

$$\dot{\mathbf{S}} = \mathbb{C} : \frac{1}{2}\dot{\mathbf{C}} + \dot{q}\frac{\partial \zeta}{\partial \mathbf{C}}, \quad \mathbb{C} = 4\frac{\partial^2 W}{\partial \mathbf{C}\partial \mathbf{C}} + 2q\frac{\partial^2 W}{\partial \mathbf{C}\partial \mathbf{C}}. \tag{10}$$

Anisotropic strain energy functions

Material symmetry

The symmetry group $\mathcal{G}$ of a material is a set of all orthogonal mappings which preserve the material symmetry. For anisotropic materials, the symmetry group can be defined with the aid of structural tensors $\mathbf{L}_i$, $i = 0,1,\ldots,n$ as

$$\mathcal{G} = \left\{ \mathbf{Q} \in \mathbf{Orth} \,:\, \mathbf{Q}\mathbf{L}_i\mathbf{Q}^{\mathrm{T}} = \mathbf{L}_i,\ i = 0, 1, \ldots, n \right\}. \tag{11}$$

For a hyperelastic material, the condition of material symmetry is written in terms of the strain energy function (5) and the symmetry group (11) by

$$W_{\mathbf{C}}(\mathbf{Q}\mathbf{C}\mathbf{Q}^{\mathrm{T}}) = W_{\mathbf{C}}(\mathbf{C}), \quad \forall \mathbf{Q} \in \mathcal{G}. \tag{12}$$

According to Rychlewski's theorem [29], this condition is satisfied if and only if the strain energy can be represented as an isotropic tensor function of arguments containing the structural tensors. In view of (11) one can thus write (see e.g., [22])

$$\begin{aligned} &W_{\mathbf{CL}}(\mathbf{Q}\mathbf{C}\mathbf{Q}^{\mathrm{T}}, \mathbf{Q}\mathbf{L}_i\mathbf{Q}^{\mathrm{T}}) = W_{\mathbf{CL}}(\mathbf{C}, \mathbf{L}_i), \\ &i = 0, 1, \ldots, n, \ \forall \mathbf{Q} \in \mathbf{Orth}. \end{aligned} \tag{13}$$

At first, we consider a general fiber-reinforced material consisting of an isotropic matrix and an arbitrary number n of fiber families as schematically shown in Fig. 1. Let the alignment direction of each fiber family be given by a unit vector $\boldsymbol{m}_i$, i = 1,2,...,n. Then we define $n + 1$ structural tensors $\mathbf{L}_i$, i = 0,1,...,n by

$$\mathbf{L}_i = \boldsymbol{m}_i \otimes \boldsymbol{m}_i, \quad \mathbf{L}_0 = \frac{1}{3}\mathbf{I}, \quad i = 1, 2, \ldots, n, \tag{14}$$

where $\mathbf{I}$ denotes the identity tensor of second order. The tensor $\mathbf{L}_0$ is assumed to be associated with the isotropic matrix. In the next step, we form linear combinations of the tensors (14) and thus define so-called generalized structural tensors by

$$\tilde{\mathbf{L}}_r = \sum_{i=0}^{n} v_i^{(r)} \mathbf{L}_i, \quad \sum_{i=0}^{n} v_i^{(r)} = 1, \quad r = 1, 2, \ldots, \tag{15}$$

where $v_i^{(r)} \geq 0$, i = 0,1,...,n denote scalar weight factors. Note that both the structural tensors (14) and the generalized structural tensors (15) are characterized by the property $\mathrm{tr}\mathbf{L}_i = \mathrm{tr}\tilde{\mathbf{L}}_r = 1, i = 0, 1, \ldots, n, r = 1, 2, \ldots$.

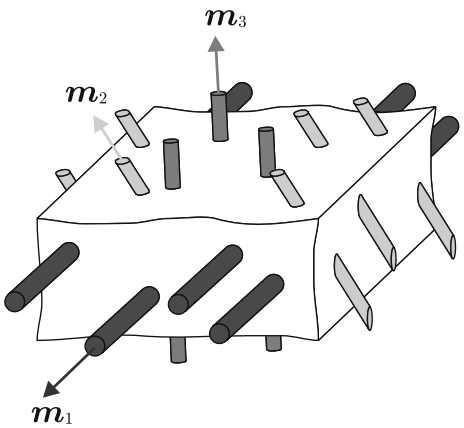

Fig. 1 General fiber-reinforced material

For orthotropic and transversely isotropic materials, another set of generalized structural tensors has recently been presented [22]. Orthotropy is characterized by symmetry with respect to three mutually orthogonal planes by reflections from which the material properties remain unchanged. The axes normal to these planes are referred to as the principal material directions. Introducing unit vectors $\boldsymbol{l}_i, i = 1, 2, 3$, in these directions allows to form the structural tensors (see e.g., [22])

$$\begin{aligned} &\widehat{\mathbf{L}}_1 = \boldsymbol{l}_1 \otimes \boldsymbol{l}_1, \quad \widehat{\mathbf{L}}_2 = \boldsymbol{l}_2 \otimes \boldsymbol{l}_2, \\ &\widehat{\mathbf{L}}_3 = \mathbf{I} - \widehat{\mathbf{L}}_1 - \widehat{\mathbf{L}}_2 = \boldsymbol{l}_3 \otimes \boldsymbol{l}_3, \end{aligned} \tag{16}$$

where a superposed hat serves to distinguish them from those associated with fiber directions (14). Transverse isotropy represents a material symmetry with respect to only one preferred direction. Rotations about this axis and reflections from planes parallel or orthogonal to it preserve the material properties. Specifying this principal material direction by a unit vector $\boldsymbol{l}_1$, two structural tensors can be defined by (see e.g., [22])

$$\widehat{\mathbf{L}}_1 = \boldsymbol{l}_1 \otimes \boldsymbol{l}_1, \quad \widehat{\mathbf{L}}_2 = \frac{1}{2}[\mathbf{I} - \mathbf{L}_1]. \tag{17}$$

In a similar manner as (15), linear combinations of the tensors (16) or (17) lead to the generalized structural tensors (cf. [22, 23])

$$\tilde{\mathbf{L}}_r = \sum_{i=1}^{m} w_i^{(r)} \widehat{\mathbf{L}}_i, \quad \sum_{i=1}^{m} w_i^{(r)} = 1, \quad r = 1, 2, \ldots, \tag{18}$$

where m = 3 for orthotropy, m = 2 for transverse isotropy and $w_i^{(r)} \geq 0$ denote scalar weight factors. In fiber-reinforced materials orthotropy and transverse isotropy arise as special cases. Indeed, certain arrangement of two or more fiber families may lead to orthotropic material symmetry and one or more fiber families aligned in one single direction result in transverse isotropy (see e.g., [30]). In this case, the generalized structural tensors defined by (15) and (18) should coincide so that consequently the weight factors $w_i^{(r)}$, i = 1,2,...,m, associated with principal material directions (16, 17) are related to the factors $v_i^{(r)}$, i = 0,1,...,n, weighting the fiber directions (14) (see Appendix).

In a recent work [12], the dispersion of collagen fibers was included into a constitutive model for arterial tissue. Therein, it is assumed that the fiber distribution is characterized by rotational symmetry about a mean preferred direction given by the unit vector $\boldsymbol{a}_0$. As a measure for the fiber distribution, a scalar parameter κ is introduced such that a so-called structure tensor $\mathbf{H}$ takes the form [12]

$$\mathbf{H} = \kappa\mathbf{I} + (1 - 3\kappa)\boldsymbol{a}_0 \otimes \boldsymbol{a}_0. \tag{19}$$

It is seen that the same form is also obtained as a special case of (15), setting $n = 1$, $\boldsymbol{m}_1 = \boldsymbol{a}_0$ and $v_0^{(r)} = 3\kappa$, which underlines the physical interpretability of the weight factors.

Functional basis

The right Cauchy–Green tensor $\mathbf{C}$ and the structural tensors (14) form a finite system of tensors. According to Hilbert's theorem, one can find a finite set of isotropic invariants V_k, $k = 1,2,...,t$ of these tensors called the functional basis, in terms of which all other isotropic invariants can be expressed. Thus in view of (13), one can write

$$W = \hat{W}(V_k), \quad k = 1, 2, \ldots, t. \tag{20}$$

Let us first consider the case where all fiber families are either parallel or mutually orthogonal. Then, taking into account the symmetry of $\mathbf{C}$ and $\mathbf{L}_i$, $i = 1,2,...,n$, and applying the classical invariant theory (see e.g., [25, 31]), a functional basis can be given by

$$\begin{gathered} V_1 = \mathrm{tr}\mathbf{C}, \quad V_2 = \mathrm{tr}\mathbf{C}^2, \quad V_3 = \mathrm{tr}\mathbf{C}^3, \\ V_{3+i} = \mathrm{tr}[\mathbf{C}\mathbf{L}_i], \quad V_{3+n+i} = \mathrm{tr}\left[\mathbf{C}^2\mathbf{L}_i\right], \quad i = 1, 2, \ldots, n, \end{gathered} \tag{21}$$

see also [30]. For a general fiber-reinforced material with arbitrary fiber alignment, the functional basis (21) is completed by the invariants

$$\mathrm{tr}\left[\mathbf{C}\mathbf{L}_i\mathbf{L}_j\right], \ \mathrm{tr}\left[\mathbf{L}_i\mathbf{L}_j\right], \ \mathrm{tr}\left[\mathbf{L}_i\mathbf{L}_j\mathbf{L}_k\right], \quad i<j<k = 1, 2, \ldots, n. \tag{22}$$

In regard to the constitutive modeling, however, it is useful to restrict the arguments of the strain energy function. The invariants $(22)_{2,3}$ are constants and will be neglected for this reason. Further, we omit the dependence of the strain energy on the coupled terms $(22)_1$ which reflect deformations of the fiber families $\boldsymbol{m}_p$ and $\boldsymbol{m}_q$ relative to each other. Accordingly, in the following, we reduce the list of arguments of the strain energy to the invariants (21) even in the case of an arbitrary fiber orientation and set $t = 3 + 2n$.

Polyconvex strain energy functions

Polyconvexity

A strain energy function $W = W_{\mathbf{F}}(\mathbf{F}) : \mathbf{Inv} \to \mathbb{R}$ is said to be polyconvex [18] if there exists a convex function $W = \breve{W}(\mathbf{F}, \mathrm{adj}\mathbf{F}, \mathrm{det}\mathbf{F}) : (\mathbf{Inv}, \mathbf{Inv}, \mathbb{R}^+) \to \mathbb{R}$ such that

$$W_{\mathbf{F}}(\mathbf{F}) = \breve{W}(\mathbf{F}, \mathrm{adj}\mathbf{F}, \mathrm{det}\mathbf{F}). \tag{23}$$

The arguments $\mathbf{F}$, adj$\mathbf{F}$ and det$\mathbf{F}$ describe the deformation of line, surface and volume elements, respectively. A subclass of polyconvex functions (23) can be obtained by the additive representation [19]

$$W_{\mathbf{F}}(\mathbf{F}) = \breve{W}_1(\mathbf{F}) + \breve{W}_2(\mathrm{adj}\mathbf{F}) + \breve{W}_3(\mathrm{det}\mathbf{F}), \tag{24}$$

where $\breve{W}_i, i = 1, 2, 3$, are convex functions of their argument, respectively.

We recall the following basic property of convex functions: Let $\varphi(\mathbf{A}) : \mathbf{Inv} \to \mathbb{R}$ be convex and $p : \mathbb{R} \to \mathbb{R}$ be convex and monotone increasing, then $p(\varphi(\mathbf{B}))$ is convex. Indeed, for some $\mathbf{B}_1, \mathbf{B}_2 \in \mathbf{Inv}$ and $\lambda \in [0, 1]$, we have

$$p(\varphi(\lambda\mathbf{B}_1 + (1-\lambda)\mathbf{B}_2)) \le p(\lambda\varphi(\mathbf{B}_1) + (1-\lambda)\varphi(\mathbf{B}_2)) \tag{25}$$

due to the convexity of φ and monotonicity of p. Since the latter is also convex we can further write

$$p(\lambda\varphi(\mathbf{B}_1) + (1-\lambda)\varphi(\mathbf{B}_2)) \le \lambda p(\varphi(\mathbf{B}_1)) + (1-\lambda)p(\varphi(\mathbf{B}_2)) \tag{26}$$

which implies convexity of $p(\varphi(\mathbf{B}))$.

Now let us consider the convexity properties of the invariants V_k, $k = 1,2,...,t$, (21), bearing in mind the requirements for polyconvex functions (23). Indeed it can be shown that the invariants V_{3+n+i}, $i = 1,2,...,n$, are not convex with respect to $\mathbf{F}$, while the remaining ones in (21) satisfy this condition [19]. However, on the basis of the Cayley–Hamilton theorem, the invariants (21) can be expressed uniquely in terms of other invariants [22]

$$\begin{gathered} I_i = \mathrm{tr}[\mathbf{C}\mathbf{L}_i], \quad J_i = \mathrm{tr}[(\mathrm{cof}\mathbf{C})\mathbf{L}_i], \quad \mathrm{III}_{\mathbf{C}} = \mathrm{det}\mathbf{C}, \\ i = 0, 1, \ldots, n, \end{gathered} \tag{27}$$

which are convex with respect to $\mathbf{F}$, adj$\mathbf{F}$ and det$\mathbf{F}$, respectively [19], and thus provide a suitable basis to formulate polyconvex functions. On account of the positive semi-definiteness of the structural tensors (14), we notice the following important property

$$I_i > 0, \quad J_i > 0, \quad i = 0, 1, \ldots, n. \tag{28}$$

The convexity properties remain unaffected by forming linear combinations of the invariants $(27)_{1,2}$ with non-negative weight factors (see e.g., [32]). Thus, in view of (15) one can define generalized invariants based on the generalized structural tensors as

$$\begin{gathered} \tilde{I}_r = \sum_{i=0}^{n} v_i^{(r)} I_i = \mathrm{tr}\left[\mathbf{C}\tilde{\mathbf{L}}_r\right], \ \tilde{J}_r = \sum_{i=0}^{n} v_i^{(r)} J_i = \mathrm{tr}\left[(\mathrm{cof}\mathbf{C})\tilde{\mathbf{L}}_r\right], \\ r = 1, 2, \ldots, \end{gathered} \tag{29}$$

which are likewise convex with respect to $\mathbf{F}$ and adj$\mathbf{F}$, respectively. The definitions (27) and (29) finally allow to represent the strain energy function in the form

$$W = \tilde{W}(\tilde{I}_r, \tilde{J}_r, \mathrm{III}_{\mathbf{C}}), \quad r = 1, 2, \ldots. \tag{30}$$

Utilizing the additive representation (24), a set of polyconvex strain energy functions can hence be constructed by

$$W = \frac{1}{4}\sum_{r=1}^{s} \mu_r \left[f_r(\tilde{I}_r) + g_r(\tilde{J}_r) + h_r\left(\mathrm{III}_{\mathbf{C}}^{1/2}\right)\right], \tag{31}$$

where $\mu_r \geq 0$ are material parameters with the dimension of stress. According to the above mentioned statement about convexity, the functions f_r and g_r are convex and monotone increasing functions of their arguments, while h_r are convex with respect to $\mathrm{III}_{\mathbf{C}}^{1/2} = \det\mathbf{F}$. The strain energy function is given in terms of a series with an arbitrary number of terms s, which offers wide flexibility in application to experimental data. Nevertheless, truncating the series after the first term, so that $s = 1$, is often sufficient to describe experimental results adequately as, e.g., shown in the numerical examples presented hereinafter.

In the next step, we consider the condition of the energy and stress free undeformed configuration. To this end, we set $\mathbf{C} = \mathbf{I}$ and require

$$W|_{\mathbf{C}=\mathbf{I}} = \frac{1}{4}\sum_{r=1}^{s} \mu_r [f_r(1) + g_r(1) + h_r(1)] = 0. \tag{32}$$

Applying (6), the condition of a stress free undeformed state reads as

$$\mathbf{S}|_{\mathbf{C}=\mathbf{I}} = 2\left.\frac{\partial W}{\partial \mathbf{C}}\right|_{\mathbf{C}=\mathbf{I}} = \frac{1}{2}\sum_{r=1}^{s} \mu_r \left\{ [f_r'(1) - g_r'(1)]\tilde{\mathbf{L}}_r + \left[g_r'(1) + \frac{1}{2}h_r'(1)\right]\mathbf{I}\right\} = \mathbf{0}. \tag{33}$$

It is observed that the hyperelastic model (31) a priori fulfills the condition of the energy and stress free undeformed configuration whenever

$$\begin{aligned} &f_r(1) = g_r(1) = h_r(1) = 0, \quad r = 1, 2, \ldots, s, \\ &f_r'(1) = g_r'(1) = -\tfrac{1}{2}h_r'(1) = 1, \quad r = 1, 2, \ldots, s. \end{aligned} \tag{34}$$

Note that the conditions (34) coincide with those imposed on the so-called generalized strain measures [33].

Equation (31) represents the natural generalization of the strain energy functions suggested in [22, 23] from two perspectives. On the one hand, the set of structural tensors (14) allows to include any fiber reinforcement geometry and thus extends the applicability of the previous model defined for orthotropic or transversely isotropic materials. On the other hand, the generalized representation (31) enables to account for various material characteristics in a straightforward manner by an appropriate choice of any convex and monotone increasing functions f_r, g_r and a convex function h_r satisfying (34). Clearly, the earlier models can be obtained as special cases. Indeed, for fiber orientations with orthotropic or transversely isotropic symmetry, the power functions

$$\begin{aligned} f_r(\tilde{I}_r) = \frac{1}{\alpha_r}\left(\tilde{I}_r^{\alpha_r} - 1\right),\ g_r(\tilde{J}_r) = \frac{1}{\beta_r}\left(\tilde{J}_r^{\beta_r} - 1\right), \\ h_r(\mathrm{III}_{\mathbf{C}}^{1/2}) = \frac{1}{\gamma_r}\left(\mathrm{III}_{\mathbf{C}}^{-\gamma_r} - 1\right) \end{aligned} \tag{35}$$

recover the strain energy proposed in [22] and showing good agreement with experiments on calendered rubber, where $\alpha_r \geq 1$, $\beta_r \geq 1$, $\gamma_r > 0$ denote material constants. Setting

$$\begin{aligned} f_r(\tilde{I}_r) = \tfrac{1}{\alpha_r}\left[e^{\alpha_r(\tilde{I}_r - 1)} - 1\right],\ g_r(\tilde{J}_r) = \tfrac{1}{\beta_r}\left[e^{\beta_r(\tilde{J}_r - 1)} - 1\right], \\ h_r(\mathrm{III}_{\mathbf{C}}^{1/2}) = \tfrac{1}{\gamma_r}\left(\mathrm{III}_{\mathbf{C}}^{-\gamma_r} - 1\right), \end{aligned} \tag{36}$$

where $\alpha_r \geq 0$, $\beta_r \geq 0$, $\gamma_r > 0$, yields the exponential model successfully utilized to describe pericardial tissue and rabbit skin in [23].

Coercivity

For the existence of a global minimizer of the total elastic energy of a body, polyconvexity of the strain energy function is not sufficient. The strain energy function additionally has to satisfy a growth condition referred to as coercivity [18, 20]. The coercivity condition can be formulated as [34, 35]

$$W(\mathbf{C}) \geq c_0[(\mathrm{tr}\mathbf{C})^p + (\mathrm{tr}(\mathrm{cof}\mathbf{C}))^q] - c_1, \ \forall \mathbf{C} \in \mathbf{S}\mathrm{ym}^+ \tag{37}$$

with real, scalar valued constants $c_0 > 0, p \geq 1, q \geq \frac{3}{4}$ and c_1. Inserting (31) into (37) one finds that (37) holds if

$$\begin{aligned} &\tfrac{1}{4}\sum_{r=1}^{s} \mu_r f_r(\tilde{I}_r) - c_0(\mathrm{tr}\mathbf{C})^p \geq d_1, \\ &\tfrac{1}{4}\sum_{r=1}^{s} \mu_r g_r(\tilde{J}_r) - c_0(\mathrm{tr}(\mathrm{cof}\mathbf{C}))^q \geq d_2, \\ &\tfrac{1}{4}\sum_{r=1}^{s} \mu_r h_r\left(\mathrm{III}_{\mathbf{C}}^{1/2}\right) \geq d_3, \end{aligned} \tag{38}$$

where $d_1 + d_2 + d_3 = -c_1$. Keeping in mind that f_r and g_r are convex, we can use the basic statement for convex functions that the first order approximation of a convex function globally underestimates the function (see e.g., [32]). Thus, expanding f_r and g_r in series around the natural

state and truncating these series after the linear term we have in consideration of (34)

$$\begin{aligned} f_r(\tilde{I}_r) &\geq f_r(1) + f_r'(1)(\tilde{I}_r - 1) = (\tilde{I}_r - 1), \\ g_r(\tilde{J}_r) &\geq g_r(1) + g_r'(1)(\tilde{J}_r - 1) = (\tilde{J}_r - 1), \quad r = 1, 2, \ldots, s. \end{aligned} \tag{39}$$

Consequently, in view of (29), the conditions $(38)_{1,2}$ are satisfied if

$$\begin{aligned} &\tfrac{1}{4}\sum_{r=1}^{s}\mu_r\left(\sum_{i=0}^{n} v_i^{(r)} I_i - 1\right) - c_0(\mathrm{tr}\mathbf{C})^p \geq d_1, \\ &\tfrac{1}{4}\sum_{r=1}^{s}\mu_r\left(\sum_{i=0}^{n} v_i^{(r)} J_i - 1\right) - c_0(\mathrm{tr}(\mathrm{cof}\mathbf{C}))^q \geq d_2. \end{aligned} \tag{40}$$

Bearing in mind $(14)_2$ and $(27)_{1,2}$ and choosing $p = q = 1$, one can rearrange the latter inequalities as

$$\begin{aligned} &\left(\tfrac{1}{12}\sum_{r=1}^{s}\mu_r v_0^{(r)} - c_0\right)\mathrm{tr}\mathbf{C} + \tfrac{1}{4}\sum_{r=1}^{s}\mu_r\left(\sum_{i=1}^{n} v_i^{(r)} I_i - 1\right) - d_1 \geq 0, \\ &\left(\tfrac{1}{12}\sum_{r=1}^{s}\mu_r v_0^{(r)} - c_0\right)\mathrm{tr}(\mathrm{cof}\mathbf{C}) + \tfrac{1}{4}\sum_{r=1}^{s}\mu_r\left(\sum_{i=1}^{n} v_i^{(r)} J_i - 1\right) - d_2 \geq 0. \end{aligned} \tag{41}$$

Taking into account the positive definiteness of I_i and J_i (28), it is seen that the conditions (41) can easily be fulfilled, setting $c_0 = 1/12\sum_{r=1}^{s}\mu_r v_0^{(r)}$ and $d_1 = d_2 = -1/4\sum_{r=1}^{s}\mu_r$. Finally, to satisfy the condition $(38)_3$ we assume the functions $h_r(\mathrm{III}_{\mathbf{C}}^{1/2})$ to be bounded below with a lower bound, say κ_r, such that

$$h_r(\mathrm{III}_{\mathbf{C}}^{1/2}) \geq \kappa_r, \quad r = 1, 2, \ldots, s, \quad \forall \mathrm{III}_{\mathbf{C}}^{1/2} \in \mathbb{R}^+. \tag{42}$$

In doing so, we find that condition $(38)_3$ is satisfied setting $d_3 = 1/4\sum_{r=1}^{s}\mu_r\kappa_r$. Thus, equations (41) and (42) imply (37).

Constitutive relations and tangent moduli

In the following, expressions for the second Piola–Kirchhoff stress and the tangent tensor are derived. Inserting the strain energy function (31) into the constitutive relation (6), the second Piola–Kirchhoff stress tensor calculates to

$$\begin{aligned} \mathbf{S} = \frac{1}{2}\sum_{r=1}^{s}\mu_r\{&f_r'(\tilde{I}_r)\tilde{\mathbf{L}}_r - g_r'(\tilde{J}_r)\mathrm{III}_{\mathbf{C}}\mathbf{C}^{-1}\tilde{\mathbf{L}}_r\mathbf{C}^{-1} \\ &+ \left[g_r'(\tilde{J}_r)\tilde{J}_r + \frac{1}{2}h_r'\left(\mathrm{III}_{\mathbf{C}}^{\frac{1}{2}}\right)\mathrm{III}_{\mathbf{C}}^{\frac{1}{2}}\right]\mathbf{C}^{-1}\Big\}. \end{aligned} \tag{43}$$

Applying the product rules of differentiation (3), the tangent tensor (8) is written as

$$\begin{aligned} \mathbb{C} = \sum_{r=1}^{s}\mu_r\Big\{&f_r''(\tilde{I}_r)\tilde{\mathbf{L}}_r \odot \tilde{\mathbf{L}}_r \\ &+ g_r''(\tilde{J}_r)\mathrm{III}_{\mathbf{C}}^2(\mathbf{C}^{-1}\tilde{\mathbf{L}}_r\mathbf{C}^{-1} \odot \mathbf{C}^{-1}\tilde{\mathbf{L}}_r\mathbf{C}^{-1}) \\ &- \left[g_r'(\tilde{J}_r) + g_r''(\tilde{J}_r)\tilde{J}_r\right]\mathrm{III}_{\mathbf{C}}(\mathbf{C}^{-1} \odot \mathbf{C}^{-1}\tilde{\mathbf{L}}_r\mathbf{C}^{-1} \\ &+ \mathbf{C}^{-1}\tilde{\mathbf{L}}_r\mathbf{C}^{-1} \odot \mathbf{C}^{-1}) \\ &+ \left[g_r'(\tilde{J}_r)\tilde{J}_r + g_r''(\tilde{J}_r)\tilde{J}_r^2 + \frac{1}{4}h_r'\left(\mathrm{III}_{\mathbf{C}}^{\frac{1}{2}}\right)\mathrm{III}_{\mathbf{C}}^{\frac{1}{2}}\right. \\ &\left. + \frac{1}{4}h_r''\left(\mathrm{III}_{\mathbf{C}}^{\frac{1}{2}}\right)\mathrm{III}_{\mathbf{C}}\right]\mathbf{C}^{-1} \odot \mathbf{C}^{-1} \\ &- \left[g_r'(\tilde{J}_r)\tilde{J}_r + \frac{1}{2}h_r'\left(\mathrm{III}_{\mathbf{C}}^{\frac{1}{2}}\right)\mathrm{III}_{\mathbf{C}}^{\frac{1}{2}}\right](\mathbf{C}^{-1} \otimes \mathbf{C}^{-1})^S \\ &+ g_r'(\tilde{J}_r)\mathrm{III}_{\mathbf{C}}(\mathbf{C}^{-1} \otimes \mathbf{C}^{-1}\tilde{\mathbf{L}}_r\mathbf{C}^{-1} + \mathbf{C}^{-1}\tilde{\mathbf{L}}_r\mathbf{C}^{-1} \otimes \mathbf{C}^{-1})^S\Big\}. \end{aligned} \tag{44}$$

In vivo, biological soft tissues contain a large amount of water and thus show a very slight compressibility. In the constitutive modeling they are often considered as incompressible. The incompressibility constraint $\mathrm{III}_{\mathbf{C}} = 1$ can be taken into account setting the constraint function ζ in (9) to

$$\zeta(\mathbf{C}) = \mathrm{III}_{\mathbf{C}}^{\frac{1}{3}} - 1. \tag{45}$$

Keeping (34) in mind, the strain energy function (31) for an incompressible material is then given by

$$W = \frac{1}{4}\sum_{r=1}^{s}\mu_r\left[f_r(\tilde{I}_r) + g_r(\tilde{K}_r)\right], \quad \tilde{K}_r = \mathrm{tr}\left(\mathbf{C}^{-1}\tilde{\mathbf{L}}_r\right), \tag{46}$$

where the invariants $\tilde{K}_r$ result from $\tilde{J}_r$ under the constraint $\mathrm{III}_{\mathbf{C}} = 1$. In this case, straightforward insertion of (45) and (46) into (9) and (10) yields the expressions for the second Piola–Kirchhoff stress tensor

$$\mathbf{S} = \frac{1}{2}\sum_{r=1}^{s}\mu_r\{f_r'(\tilde{I}_r)\tilde{\mathbf{L}}_r - g_r'(\tilde{K}_r)\mathbf{C}^{-1}\tilde{\mathbf{L}}_r\mathbf{C}^{-1}\} + \frac{1}{3}q\mathbf{C}^{-1}, \tag{47}$$

and the tangent tensor of fourth order

$$\begin{aligned} \mathbb{C} = \sum_{r=1}^{s}\mu_r\Big\{&f_r''(\tilde{I}_r)\tilde{\mathbf{L}}_r \odot \tilde{\mathbf{L}}_r + g_r''(\tilde{K}_r)(\mathbf{C}^{-1}\tilde{\mathbf{L}}_r\mathbf{C}^{-1} \odot \mathbf{C}^{-1}\tilde{\mathbf{L}}_r\mathbf{C}^{-1}) \\ &+ g_r'(\tilde{K}_r)(\mathbf{C}^{-1} \otimes \mathbf{C}^{-1}\tilde{\mathbf{L}}_r\mathbf{C}^{-1} + \mathbf{C}^{-1}\tilde{\mathbf{L}}_r\mathbf{C}^{-1} \otimes \mathbf{C}^{-1})^S \\ &+ \frac{2}{3}q\left[\frac{1}{3}\mathbf{C}^{-1} \odot \mathbf{C}^{-1} - (\mathbf{C}^{-1} \otimes \mathbf{C}^{-1})^S\right]\Big\}. \end{aligned} \tag{48}$$

Numerical examples

In this section, the constitutive model (31) is specified and applied to two different sets of experimental data on human arterial tissue. Arteries are composed of three distinct layers called intima, media and adventitia. In constitutive modeling, each layer is often considered as an incompressible fiber-reinforced composite with two mechanically equivalent families of collagen fibers that form symmetrical helices tilted by an angle $\pm\varphi$ against the circumferential direction [4, 13, 36].

Coronary arteries

In a recent work, Holzapfel et al. [36] have studied the layer-specific mechanical properties of human coronary arteries with non-atherosclerotic intimal thickening in cyclic uniaxial quasi-static tension tests. Therein, strips from left anterior descending coronary arteries were split into the adventitial, medial and intimal layer and finally loaded such that the principal axes of deformation coincided with the circumferential, axial and radial direction of the vessel. For each strip sample, the recorded stress response for loading in circumferential and axial direction was modeled using a hyperelastic constitutive model based on the above mentioned fiber-reinforcement assumption (see [36] for details).

In order to describe the mechanical behavior of the arterial tissue samples, we first specialize the polyconvex strain energy function (31). To this end, we choose appropriate formulations for the functions f_r, g_r and h_r. For all three arterial layers, a clearly exponential shape of the stress-stretch curves is observed and thus the representation (36) appears to be suitable. Furthermore, we assume that each layer can be described as an incompressible reinforced material with two equivalent families of fibers arranged by an angle $\pm\varphi$ as described above. Introducing unit vectors $\boldsymbol{e}_\theta$ and $\boldsymbol{e}_z$ in the circumferential and axial direction of the artery, respectively, the orientations of the two fiber families are given by the vectors

$$\boldsymbol{m}_1 = \cos\varphi\boldsymbol{e}_\theta + \sin\varphi\boldsymbol{e}_z, \quad \boldsymbol{m}_2 = \cos\varphi\boldsymbol{e}_\theta - \sin\varphi\boldsymbol{e}_z. \tag{49}$$

Applying formulae (14, 15, 29, 46_2) and taking into account the mechanical equivalence of the fiber families, so that $v_2^{(r)} = v_1^{(r)}$, one obtains the generalized invariants

$$\begin{aligned}\tilde{I}_r &= \tfrac{1}{3}\left(1-2v_1^{(r)}\right)\left(\lambda_\theta^2+\lambda_z^2+(\lambda_\theta\lambda_z)^{-2}\right)\\ &\quad +2v_1^{(r)}\left(\lambda_\theta^2\cos^2\varphi+\lambda_z^2\sin^2\varphi\right),\\ \tilde{K}_r &= \tfrac{1}{3}\left(1-2v_1^{(r)}\right)\left(\lambda_\theta^{-2}+\lambda_z^{-2}+(\lambda_\theta\lambda_z)^{2}\right)\\ &\quad +2v_1^{(r)}\left(\lambda_\theta^{-2}\cos^2\varphi+\lambda_z^{-2}\sin^2\varphi\right),\end{aligned} \tag{50}$$

where λ_θ and λ_z denote the principal stretches in circumferential and axial direction, respectively. Furthermore, the incompressibility constraint $\lambda_\theta\lambda_z\lambda_r = 1$ has been taken into account, where λ_r denotes the radial stretch. Considering one single term $s = 1$ in the series representation (46) we have in view of (36) (cf. [23])

$$\bar{W} = \frac{\mu}{4}\left\{\frac{1}{\alpha}\left[\exp\left\{\alpha\left(\tilde{I}-1\right)\right\}-1\right]+\frac{1}{\beta}\left[\exp\left\{\beta\left(\tilde{K}-1\right)\right\}-1\right]\right\}, \tag{51}$$

where the index "1" has been omitted for the sake of clarity and $\tilde{I}$ and $\tilde{K}$ are given by (50). Note that by this means, we reduce the set of unknown material constants to μ,α,β,v_1 and the angle φ. With these results at hand, and assuming that the lateral directions are stress free in the uniaxial tension test, the Cauchy stresses in circumferential and axial direction are calculated, respectively, by

$$\sigma_\theta = \lambda_\theta\frac{\partial\bar{W}}{\partial\lambda_\theta}, \quad \sigma_z = \lambda_z\frac{\partial\bar{W}}{\partial\lambda_z}. \tag{52}$$

This model was fitted and compared to the experimental results from one sample (*specimen IX* in [36]). In this way, the parameters μ,α,β,v_1 and φ were determined for each layer, where φ was likewise treated as a phenomenological parameter regardless of its physical interpretability. The experimental and model results are presented as Cauchy stress versus stretch diagrams in Fig. 2 together with the values of the material parameters. For all three layers accurate agreement is observed.

Abdominal aorta

Vande Geest et al. [37] have studied the age dependency of the mechanical behavior of the human abdominal aorta in biaxial tension-controlled tests. To this end, infrarenal abdominal aortic square samples were biaxially loaded in circumferential and axial direction. Different protocols varying in the ratio between circumferential and axial tension, $T_{\theta\theta}$:T_{zz}, were applied (see [37] for details). An interesting result is the difference in the form of the stress responses of samples obtained from different age groups. Given as second Piola–Kirchhoff stress versus Green–Lagrange strain, the curves change from a sigmoidal shape in the youngest group (<30 years) to an exponential nature in the older ones. As no data on the single layers of the arteries are available, we consider the whole artery as an incompressible fiber-reinforced material with two symmetrically arranged fiber helices as described above for the single layers. Thus, assuming that the principal axis of deformation coincide with the circumferential, axial and radial direction, the fiber orientation and generalized

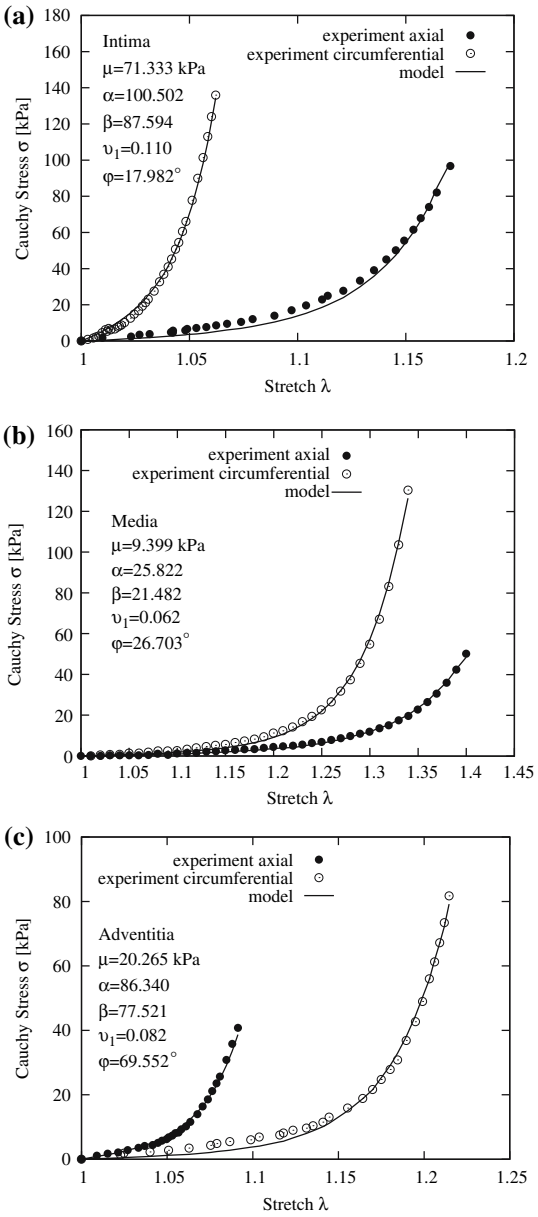

Fig. 2 Comparison of the polyconvex model (51) with experimental data on coronary artery layers [36]

invariants are again calculated according to (49) and (50). In particular, we focus on the stress response of the young arteries. Their *s*-shaped stress-strain curves show a noticeable similarity to those obtained in experiments with rubber materials (see e.g., [38]). For this reason, we choose the functions f_r and g_r in a logarithmic form motivated by the Gent model for rubber elasticity [39]. Setting $s = 1$ in (36), this leads to

$$\bar{W} = \frac{\mu}{4}\left\{-\alpha \ln\left(1 - \frac{\tilde{I} - 1}{\alpha}\right) - \beta \ln\left(1 - \frac{\tilde{K} - 1}{\beta}\right)\right\}, \qquad (53)$$

wherein $\alpha > 0$, $\beta > 0$ are material parameters determining the limiting values of $\tilde{I} - 1$ and $\tilde{K} - 1$, respectively. Assuming that the radial direction is stress free, the second Piola–Kirchhoff stresses in circumferential and axial direction can be calculated, respectively, by

$$S_\theta = \lambda_\theta^{-1} \frac{\partial \bar{W}}{\partial \lambda_\theta}, \quad S_z = \lambda_z^{-1} \frac{\partial \bar{W}}{\partial \lambda_z}. \qquad (54)$$

We fitted the model (53) to the results of the test protocols with $T_{\theta\theta}$:T_{zz} ratios 0.5:1, 1:1, and 1:0.5, considering *specimen 3* in [37]. The results are shown in Fig. 3 together with the data obtained from the plots in [37]. In the next step, the parametrized model was used to predict the stress in circumferential and axial direction for the remaining protocols 0.75:1 and 1:0.75. The simulated as well as the experimental values are presented in Fig. 4 and show good agreement.

In both examples, identification of the material parameters was achieved by means of least-squares and a Levenberg–Marquardt type algorithm. It should be noted that the experimental data was obtained from printed diagrams which might have led to some slight inaccuracies.

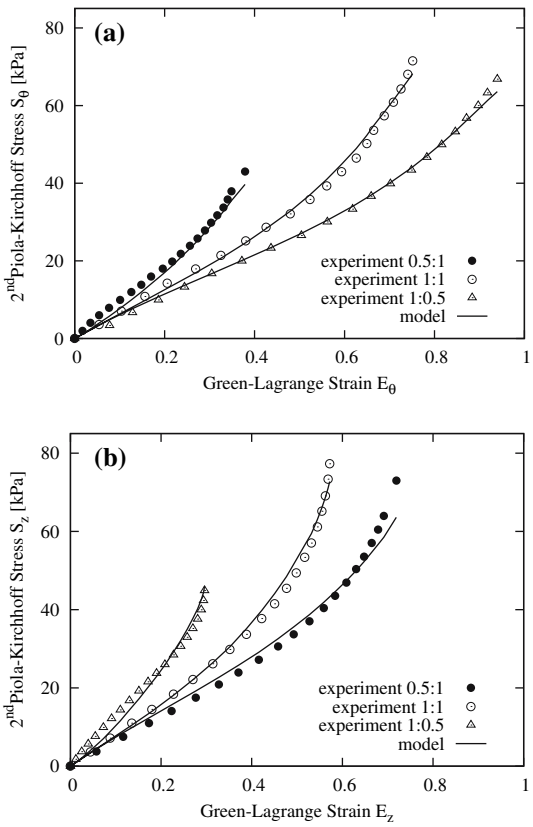

Fig. 3 Comparison of the polyconvex model (53) with experimental data [37]. Material constants: $\mu = 81.048$ kPa, $\alpha = 2.060$, $\beta = 0.408$, $\nu_1 = 0.498$, $\varphi = 47.59°$

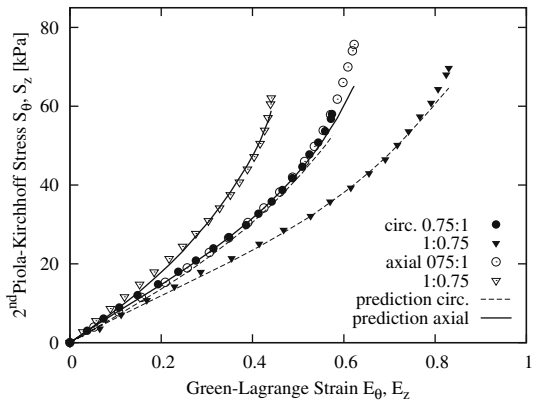

Fig. 4 Experimental data [37] and prediction by the polyconvex model (53)

These are, however, considered negligible in comparison to the variation in data among individual tissue samples.

Conclusions

In the present paper we have presented a generalized polyconvex and coercive strain energy function for fiber-reinforced materials. The model is able to take into account the collagen fiber structure of soft biological tissues. The strain energy function is given in a generalized form offering wide flexibility in application to different types of tissue. For example, the model agreed appropriately with the mechanical behavior of arterial tissue in various experiments. The agreement was achieved with a small number of material constants, some of which allow for a physical interpretation. Further, the model adequately predicted the stress response for loading conditions which had not been considered for parameter identification. As a result of polyconvexity and coercivity the model is elliptic for all admissible strains and guarantees the existence of a solution of a boundary value problem.

As previously mentioned, the mechanical characteristics vary among different kinds of tissue. For this reason, further evaluation of the capacities of the model in application to other tissue types and various test protocols might be useful and is going to be conducted.

Appendix

Relations between the generalized structural tensors (15) and (18)

In the following, the relations between the weight factors $w_i^{(r)}$, $i = 1,...,n$, associated with principal material directions (18) and the factors $v_i^{(r)}$, $i = 0,1,...,n$, related to matrix and fibers (15) are given for some basic fiber constellations.

Unidirectional alignment of one family of fibers leads to transverse isotropy with respect to the fiber direction. Setting $n = 1$ in $(15)_1$ and insertion of $(14)_1$, $(15)_2$ leads in view of $(17)_2$ to

$$\tilde{\mathbf{L}}_r = v_0^{(r)}\mathbf{L}_0 + v_1^{(r)}\mathbf{L}_1 = \frac{1}{3}\left(1 - v_1^{(r)}\right)\mathbf{I} + v_1^{(r)}\mathbf{L}_1 = \frac{1}{3}\left(1 + 2v_1^{(r)}\right)\widehat{\mathbf{L}}_1 + \frac{2}{3}\left(1 - v_1^{(r)}\right)\widehat{\mathbf{L}}_2.$$

In a fiber reinforced material, orthotropy may be the result of different fiber configurations. We first consider the case where fibers are aligned in three mutually orthogonal fiber directions coinciding with the principal material directions, so that $\boldsymbol{l}_i = \boldsymbol{m}_i, i = 1,2,3$. Then, in view of (15,16,18) one obtains

$$\tilde{\mathbf{L}}_r = \frac{1}{3}\sum_{i=1}^{3}\left[1 - v_1^{(r)} - v_2^{(r)} - v_3^{(r)} + 3v_i^{(r)}\right]\widehat{\mathbf{L}}_i.$$

A material with two orthogonal fiber families is likewise orthotropic, where the principal directions are given by the two fiber directions, so that $\boldsymbol{l}_1 = \boldsymbol{m}_1$ and $\boldsymbol{l}_2 = \boldsymbol{m}_2$, and the direction normal to the plane in which the fibers lie. The generalized structural tensors (18) are thus given by

$$\tilde{\mathbf{L}}_r = \frac{1}{3}\left[1 + 2v_1^{(r)} - v_2^{(r)}\right]\widehat{\mathbf{L}}_1 + \frac{1}{3}\left[1 - v_1^{(r)} + 2v_2^{(r)}\right]\widehat{\mathbf{L}}_2 + \frac{1}{3}\left[1 - v_1^{(r)} - v_2^{(r)}\right]\widehat{\mathbf{L}}_3.$$

Two equivalent families of fibers ($v_2^{(r)} = v_1^{(r)}$) aligned in two arbitrary directions result in orthotropy. The principal material directions are given by the bisectors of the two fiber directions and the normal to the plane in which the fibers lie. The fiber directions can be expressed in terms of the principal material directions by

$$\boldsymbol{m}_1 = \cos\alpha\,\boldsymbol{l}_1 + \sin\alpha\,\boldsymbol{l}_2,\ \boldsymbol{m}_2 = \cos\alpha\,\boldsymbol{l}_1 - \sin\alpha\,\boldsymbol{l}_2,$$

where the angle between the fibers is 2α. Hence, the generalized structural tensors read as

$$\tilde{\mathbf{L}}_r = \frac{1}{3}\left[1 + (6\cos^2\alpha - 2)v_1^{(r)}\right]\widehat{\mathbf{L}}_1 + \frac{1}{3}\left[1 + (6\sin^2\alpha - 2)v_1^{(r)}\right]\widehat{\mathbf{L}}_2 + \frac{1}{3}\left[1 - 2v_1^{(r)}\right]\widehat{\mathbf{L}}_3.$$

Finally, if there is a third fiber family $i = 3$ aligned normal to the plane spanned by the mechanically equivalent fiber families, we have

$$\tilde{\mathbf{L}}_r = \frac{1}{3}\left[1 + (6\cos^2\alpha - 2)v_1^{(r)} - v_3^{(r)}\right]\widehat{\mathbf{L}}_1 + \frac{1}{3}\left[1 + (6\sin^2\alpha - 2)v_1^{(r)} - v_3^{(r)}\right]\widehat{\mathbf{L}}_2 + \frac{1}{3}\left[1 - 2v_1^{(r)} + 2v_3^{(r)}\right]\widehat{\mathbf{L}}_3.$$

Additionally, superposition of several of the given cases may preserve the orthotropic material symmetry.

References

1. Humphrey JD (2002) Cardiovascular Solid mechanics: cells, tissues, and organs. Springer, New York
2. Fung YC (1993) Biomechanics mechanical properties of living tissues, 2nd ed. Springer, New York
3. Sacks MS (2000) J Elasticity 61:199
4. Holzapfel GA, Gasser TC, Ogden RW (2000) J Elasticity 61:1
5. Schmid H, Nash MP, Young AA, Hunter PJ (2006) ASME J Biomech Eng 128:742
6. Arruda EM, Boyce MC (1993) J Mech Phys Solids 41:389
7. Bischoff JE, Arruda EA, Grosh K (2002) J Appl Mech 69:570
8. Kuhl E, Garikipati K, Arruda EM, Grosh K (2005) Mech Phys Solids 53:1552
9. Lanir Y (1978) Biophys J 24:541
10. Kastelic J, Palley I, Baer E (1980) J Biomech 13:887
11. Freed AD, Doehring TC (2005) ASME J Biomech Eng 127:587
12. Gasser TC, Ogden RW, Holzapfel GA (2006) J R Soc Interface 3:15
13. Holzapfel GA, Gasser TC, Ogden RW (2004) ASME J Biomech Eng 126:264
14. Merodio J, Ogden RW (2002) Arch Mech 54:525
15. Merodio J, Ogden RW (2003) Int J Solids Struct 40:4707
16. Wilber JP, Walton JR (2002) Math Mech Solids 7:217
17. Chuong CJ, Fung YC (1983) ASME J Biomech Eng 105:268
18. Ball JM (1977) Arch Rat Mech Anal 63:337
19. Schröder J, Neff P (2003) Int J Solids Struct 40:401
20. Ball JM (2002) Geometry, mechanics, and dynamics. Springer, New York, p 3
21. Steigmann DJ (2003) Math Mech Solids 8:497
22. Itskov M, Aksel N (2004) Int J Solids Struct 41:3833
23. Itskov M, Ehret AE, Mavrilas D (2006) Biomech Model Mechanobiol 5:17
24. Balzani D, Neff P, Schröder J, Holzapfel GA (2006) Int J Solids Struct 43:6052
25. Itskov M (2007) Tensor algebra and tensor analysis for engineers with application to continuum mechanics. Springer, Berlin
26. Itskov M (2002) ZAMM 82:535
27. Truesdell C, Noll W (1965) Handbuch der Physik, vol III/3. Springer, Berlin
28. Ogden RW (1984) Non-linear elastic deformations. Ellis Horwood, Chichester
29. Zhang JM, Rychlewski J (1990) Arch Mech 42:267
30. Spencer AJM (1984) Continuum theory of the mechanics of fibre-reinforced composites. Springer Wien, p 1
31. Boehler JP (1977) ZAMM 57:323
32. Boyd S, Vandenberghe L (2004) Convex optimization. Cambridge University Press, Cambridge
33. Hill R (1968) J Mech Phys Solids 16:229
34. Müller S, Qi T, Yan BS (1994) Ann Inst Henri Poincaré Analyse non linéaire 11:217
35. Ball JM (1996) Bull Amer Math Soc 33:269
36. Holzapfel GA, Sommer G, Gasser CT, Regitnig P (2005) Am J Physiol Heart Circ Physiol 289:2048
37. Vande Geest JP, Sacks MS, Vorp DA (2004) ASME J Biomech Eng 126:815
38. Treloar LRG (1975) The physics of rubber elasticity, 3rd ed. Oxford University Press
39. Gent A (2004) Rubber Chem Technol 96:59